Upper Tropospheric Humidity Algorithm Assessment

Darren L. Jackson

Cooperative Institute for Research in Environmental Sciences

University of Colorado, Boulder, Colorado

Darren.L.Jackson@noaa.gov

John J. Bates

NOAA Environmental Technology Laboratory, Boulder, Colorado

Revisions completed 6/29/01 for

Journal of Geophysical Research

Abstract

This study assesses a common analytic expression used to compute upper tropospheric humidity (UTH) from satellite brightness temperatures at 6.7 μm. Vertical averaging methods for UTH were found to have significant impact on the algorithm. The temperature lapse parameter, β, had more latitudinal variance than previously found; however, large vertical gradients in mid-latitude profiles degraded UTH retrievals. The scaled reference pressure parameter, P_0, did sufficiently improve the radiance-to-humidity relationship with exception to mid-latitude profiles where P_0 exceeds 1.7. A new method for computing the reference pressure parameter is presented using HIRS channel 6 observations. Error analysis of radiance-to-humidity relationship indicates absolute UTH errors increase with increasing humidity with largest errors of 15 % per 1 K bias between simulated and observed brightness temperatures.

1. Introduction

The term upper tropospheric humidity (UTH) refers to a layer-averaged (300-500 hPa) relative humidity computed from polar-orbiting or geostationary satellite observations at water vapor channels near 6.7 μm. Because UTH is derived from satellite radiance (or brightness temperature, the terms are used interchangeably in this paper), differing assumptions about the radiance-to-humidity relationship can produce significant biases between methods. In this study, we examine the strengths and weaknesses of the various assumptions used in the relationship between UTH and satellite radiance.

While several studies use inversion methods from which to retrieve water vapor using infrared satellite observations (Susskind et al., 1997; Chaboureau et al., 1998), Soden and Bretherton (1993) first introduced the UTH method analyzed in this study. The advantage to their method was to provide a more easily understood interpretation of the satellite water vapor radiance for model evaluation and diagnostic studies. Their method also eliminated a full retrieval so to improve computational speed in transforming brightness temperature to relative humidity. Subsequent papers refined the method (Soden and Bretherton, 1996; Stephens et al., 1996), verified results with *in situ* data (Soden et al., 1994), compared results with GCM output (Bates and Jackson, 1997; Soden and Bretherton, 1994), and examined climate processes and variability (Bates et al., 2001; Jedlovec et al., 2000; Spencer and Braswell, 1997; Soden and Fu, 1995; Schmetz et al., 1995). Stephens et al. (1996) refinement of the UTH equation emphasized the importance for considering the water vapor continuum rather than just lines in the forward radiative transfer model and emphasized the use of temperature lapse rate information rather than reference pressure information.

In this paper we provide a more complete assessment of UTH. In section 2, we summarize the tradeoffs that arise due to differing assumptions about what parameters need to be accounted for in the radiance-to-humidity relationship. In section 3, we examined the characteristics of the vertical temperature and moisture profiles for tropical and mid-latitude climate zones. We assess the impact various assumptions and climate zones have on the UTH algorithm in section 4. We introduce a UTH algorithm for HIRS

observations by using an optimum satellite temperature channel to predict the reference pressure in section 5. We then summarize the results of our study in section 6.

2. UTH Methodology

Soden and Bretherton (1993) derived a relation between UTH and 6.7 μm brightness temperature using

$$a + bT_{6.7} = Ln\left(\frac{< RH > P_0}{\beta \cos\theta}\right) \quad (1)$$

where $T_{6.7}$ is the observed 6.7 μm brightness temperature (HIRS channel 12 is used in this paper but water vapor channels found on other satellites could apply), <RH> is the vertically integrated relative humidity (or UTH), P_0 (=P[T= $T_{6.7}$]/300 hPa) is the scaled reference pressure, β (=<P/T dT/dp>) is the vertically integrated dimensionless lapse rate parameter, θ is the satellite view angle, and coefficients *a* and *b* are fitted parameters. Moisture variations contribute most of the variance in $T_{6.7}$; however, variations due to temperature become significant in the mid-latitudes. Two temperature dependent parameters found in (1) are P_0 and β. P_0 represents the pressure where the temperature equals $T_{6.7}$ and is approximated by assuming the mean $T_{6.7}$ = 240 K. P_0 accounts for latitudinal changes in upper tropospheric temperature. β accounts for changes in the temperature lapse rate and generally decreases poleward in the upper troposphere since the tropopause descends from the equator to the poles.

Evolution of the UTH algorithm has seen discrepancies in using these temperature dependent parameters. Soden and Bretherton (1993) originally found variations in both P_0 and β to not significantly reduce the scatter in (1) so they ignored the contribution from these parameters. However, Soden and Bretherton (1996) later found P_0 variations to significantly improve the radiance-to-humidity relationship, yet they did not include β since its latitudinal variance was found to be five times less than P_0. Stephens et al. (1996) removed P_0 from their UTH derivation by assuming only overburden above P_0 and included β since they found a linear relationship with the difference in HIRS temperature channels 4 and 6. Stephens et al. (1996) also used the transmission function to compute vertical averages for <RH> and β instead of using a UTH weighting profile sensitive to changes in relative humidity as is done in Soden and Bretherton (1996).

3. Profile analysis of UTH parameters

Regression coefficients for the UTH algorithm were derived from the TOVS Initial Guess Retrieval (TIGR)-3 data set (Chaboureau et al., 1998). The TIGR-3 data set is a diverse set of 2311 radiosonde profiles designed to capture a wide range of atmospheric temperature and moisture profiles. The profiles are divided into five climate zones: 872 tropical profiles (TROP), 388 warm mid-latitude profiles (MIDL-1), 354 cold mid-latitude profiles (MIDL-2), and two polar zones. The warm mid-latitude profiles are located closer to the tropics, whereas cold mid-latitude profiles are located closer to the polar regions. We only used the tropical and two mid-latitude climate regimes, since the observed water vapor signal is too small for reliable retrievals of UTH in the polar

regions. The simulated NOAA-7 HIRS channel 12 brightness temperatures and transmission functions were produced using MODTRAN 3.7 (Berk et al., 1989; Wang et al., 1996). Simulations using NOAA-7 instrument parameters are used because the HIRS observations were intercalibrated to this satellite (Bates et al., 1996). All parameters from (1) were derived for each profile and the vertically averaged parameters were computed using both transmission and UTH weighting functions (hereafter referred to as transmission weights and UTH weights). The HIRS channel 12 transmission function is defined through the radiative transfer equation for cloud-free conditions and no surface reflection

$$I_\nu = B_\nu(T_s)\tau_\nu(p_s,0) + \int_{p_s}^{0} B_\nu(T(p))\frac{d\tau_\nu(p,0)}{dp}dp \qquad (2)$$

where I_ν is the upwelling spectral radiance seen by satellite, B indicates blackbody radiance, τ represents transmittance, and $d\tau/dp$ gives the rate of change in transmission of IR radiation as function of pressure. The first term represents the radiance emitted from the surface and the second term represents the radiance emitted by the atmosphere. Absorber amount and path length affects the transmission while the temperature and transmission profiles affect brightness temperatures. Transmission functions ($d\tau/dLnp$) at this wavelength can peak from 300 to 700 hPa depending on the vertical profile of water vapor and temperature. Soden and Bretherton (1996) use temperature as the vertical coordinate and compute weights based on the sensitivity of $T_{6.7}$ on relative humidity. These weights are given in Table 1. We compare the effects on a number of different

parameters using either the UTH weights (denoted by subscript U) or transmission weights (denoted by subscript T). Vertically dependent quantities were computed at each TIGR-3 pressure level.

First step in our analysis was to examine the vertical distribution of T, RH, β, and the UTH and transmission weights for the TIGR-3 tropical and mid-latitude profiles. Figures 1 through 5 give the mean and standard deviation profile for three TIGR-3 climate zones for each of these parameters along with the vertically averaged values using both the UTH and transmission weights. The UTH weights (figure 1) and the transmission weights (figure 2) were normalized for each profile to a maximum value of unity to facilitate comparison. The largest difference between transmission and UTH weights occurs for mid-latitude profiles where the UTH weighting profile is broader. Large differences in the standard deviation for these profiles occur in the tropics. This behavior in the tropics will later prove to be decisive in increasing the scatter when fitting the satellite observations to the profile data. Horizontal lines on figures 1 and 2 indicate the mean and standard deviation of P_0. The standard deviation increases and the level lowers for increasing latitude indicating that mid-latitude profiles exhibit more temperature variability. The mean corresponds well with the mean peak in both weighting profiles. Figure 3 gives the mean temperature sounding for each climate zone. Generally the temperature lapse rate (dT/dp) in the upper troposphere decreases with latitude. Temperatures become cooler and the tropopause clearly descends to near 300 hPa for the MIDL-2 profiles. The lapse rate decreases for the mid-latitude profiles along with the height of the 240 K isotherm. This reduction in temperature gradient causes the broader

mid-latitude weighting profiles seen in Figures 1 and 2. Figure 4 shows the mean relative humidity to be nearly invariant in the vertical for the tropical profiles; however, this region has the highest standard deviation. The vertical gradient increases for the mid-latitude profiles and increases significantly in the tropopause. Figure 5 shows β varies significantly in the upper tropospheric mid-latitude profiles. β decreases significantly approaching the tropopause and tends to maximize near the peak of the weighting functions.

Based on the results of figures 4 and 5, <RH> and β have the smallest vertical variation in the tropics and are more highly variant for the average mid-latitude profile. In particular, changes in β become large in the upper troposphere of the mid-latitude profiles. When combined with the broader UTH weighting profile, β_U is less than β_T in the mid-latitudes. Also, figure 5 suggests that latitudinal variations in β_T are larger than are indicated in figure 2 of Soden and Bretherton (1996). The relative change of $\pm$15% in β_T from TROP to MIDL-2 climate zones is three times higher than the $\pm$ 5% given in Soden and Bretherton (1996). Differences between these results are likely due to differences in the profile data sets. The TIGR-3 data set explicitly isolates a wide range of profile types while Soden and Bretherton (1996) used ECMWF analysis that may contain a large percentage of profiles with similar characteristics. Variations in P_0 between the same zones are $\pm$22% which compares favorably with $\pm$25% reported in Soden and Bretherton (1996).

4. Analysis of UTH least squares fit

The purpose for (1) is to have a simple equation relating $T_{6.7}$ to UTH. To accomplish this task, coefficients *a* and *b* were computed by least squares fit using simulated HIRS channel 12 brightness temperatures (T_{H12}) and computed variables β, P_0, and <RH> from the TIGR-3 profiles.

Figure 6 is a plot of scattergrams of T_{H12} versus Ln(UTH) using both forms of vertical averaging and separating profiles by climate type. The difference between the vertical averaging methods is greatest for the driest tropical profiles seen in Figures 6a and 6b (ie. the highest brightness temperatures). Much of the large scatter and wet bias in $<RH>_T$ is caused by the sensitivity of the transmission function to changes in water vapor for tropical profiles. Extremely dry profiles appear wetter using the transmission weights because rapid changes in specific humidity in the lower troposphere and a dry upper troposphere are misinterpreted as higher UTH. Figure 7 gives an example of how the UTH and transmission weights differ for an extremely dry profile. The weights for figure 7a indicate little difference in vertical structure, so the UTH values are almost identical for this relatively wet profile. However, figure 7b indicates a large separation in the peak of the weighting profiles with the transmission weights peaking much lower in the troposphere. The humidity profile in figure 7b is near 70% up to 800 hPa but reduces to values below 2% for all levels above 800 hPa. Such extremely dry profiles result in an overestimation of the UTH value using the transmission weights and degrade the radiance-to-humidity relationship in figure 6b. Figures 1a and 2a show a significant difference in the standard deviation between UTH and transmission weights for tropical

profiles. The higher standard deviation for tropical transmission functions shown in figure 2a results in the larger radiance-to-humidity scatter seen in Figure 6b. The fit for profiles outside of the tropics (Figure 6c-f) is very close between the two averaging methods with a slightly tighter fit for $<RH>_T$ for the coldest (wettest) profiles. Certainly, figure 6 indicates substantial improvement in the fit by using the UTH weights in the tropical atmospheres. The three climate zones show a notable offset in relationship between T_{H12} and UTH (Figure 6g and h). For a given value of UTH, the MIDL-2 profiles have lower T_{H12} values than its tropical counterpart. This difference indicates the background temperature is lower for the MIDL-2 profiles and reduces the T_{H12} by 5 K from a typical tropical profile with the same UTH.

Figure 8 compares two different UTH methods presented in the literature. Method 1 fits T_{H12} to $Ln(UTH/\beta)$ as was done in Stephens et al. (1996), whereas method 2 fits T_{H12} to $Ln(UTH \cdot P_0)$ as was done in Soden and Bretherton (1996). Both methods use UTH weights for vertical averaging based on the results in figure 6. The radiance-to-humidity fit improves for both methods using the tropical profiles as is indicated by a reduction in rms error in figures 8a and 8b to figure 6a. However, the MIDL-1 case shows increased rms error for both methods and the MIDL-2 case shows much greater rms error for method 1. The large scatter for the method 1 in the MIDL-2 case can be attributed to the strong vertical temperature gradient for these profiles and the relative low values caused by a lower tropopause. Therefore, the assumption of a vertically invariant β breaks down for the MIDL-2 profiles. The rms error for all profiles (figures 8g-h) is signficantly lower for method 2 due to the problem with β for MIDL-2 profiles. The method 2 results in

figure 8h are substantially better than figure 6g because P_0 accounts for changes in the temperature field between climate zones. The variance in coefficients *a* and *b* between the different climate zones for method 2 is much smaller in figure 8 than figure 6.

5. HIRS UTH retrieval

An optimized UTH retrieval is developed for HIRS observations so to have a self-consistent UTH algorithm for HIRS observations. Our proposed method gives instantaneous values for P_0 as opposed to monthly mean values used by Soden and Bretherton (1996), and screens those profiles with temperature profiles outside the acceptable range for a valid UTH retrieval.

5.1 Reference pressure method

A method for estimating P_0 is required for computing UTH. Soden and Bretherton (1996) estimate P_0 by using a monthly climatology based on ECMWF temperature data. HIRS observations, however, provide temperature soundings from channels that sense CO_2 emission in the 15-μm region (channels 1-8). In this discussion we utilize HIRS channels 4 and 6 (T_{H4} and T_{H6} respectively) to observe layer mean temperatures centered at 400 and 800 hPa respectively.

The reference pressure P_0 tends to increase poleward as the 240 K isotherm lowers with the tropopause. Figure 1 shows how the MIDL-2 profiles have a mean P_0 value near 1.6

and the variance increases significantly for these cold mid-latitude profiles. Figure 4 shows how the mean relative humidity lapse rate at upper levels for MIDL-2 profiles diverge from zero thus giving additional error to the UTH retrieval. Therefore, a threshold method for screening these undesirable profiles was developed by considering the difference between T_{H4} and T_{H6}. This difference can loosely be interpretted as identifying the temperature lapse rate of the middle troposphere. Figure 9 gives this difference as a function of TIGR-3 profile. The difference is largest for the tropical profiles since no intrusion from the tropopause is evident in channel 4 observations thus making the temperature lapse rate largest for these profiles (see figure 3). Choosing 20 K as the threshold preserves all the tropical profiles, eliminates a few MIDL-1 profiles, and removes nearly all MIDL-2 profiles.

Using this threshold method, we performed a best fit to T_{H6} with the computed P_0 from the TIGR-3 profiles. Simulations for these two channels were performed using OPTRAN (McMillin et al., 1995) since its simulations of these temperature channels compares more favorably to line-by-line models than MODTRAN (Garand et al., 2000). The linear fit is characterized by the following expression

$$P_H = a + bT_{H6} \tag{3}$$

where P_H is the fitted scaled reference pressure using HIRS observations and *a* and *b* are the fitted parameters. Figure 10a shows a good linear fit using the TIGR-3 profiles with T_{H6}-T_{H4} > 20 K and rms error is less than 0.1 whereas figure 10b indicates significant scatter for the T_{H6}-T_{H4} < 20 K profiles with rms error almost double the results in figure

10a. For the results in figure 10b, P_0 values less than 1.0 and T_{H6} values between 250-255 K indicate mid-latitude profiles with a relatively small temperature lapse rate, whereas P_0 values near 2.0 indicate cold profiles where 240 K isotherm extends below 500 hPa. Both profile types should be removed from a UTH retrieval.

Channel 6 had better correlation and RMS error than both channels 4 and 5. This result may not be intuitive since a typical weighting function for channel 6 peaks near 800 hPa whereas channels 4 and 5 peak at 400 and 600 hPa respectively. However, since the weighting profiles for these channels are so broad, the relatively cold mid-latitude profiles have the tropopause intrude in channels 4 and 5 brightness temperatures thus contaminating results for the relatively cold profiles.

5.2 Reference pressure comparison

We performed a comparison between the scaled reference pressure parameter derived from ECMWF forecast model data and those computed from the HIRS channel 6 data. Soden and Bretherton (1996) computed monthly-mean maps from five years of data. We computed pentad maps of P_H using the method described in section 5.1 and then constructed monthly climatologies using the 20-yr period of HIRS data. Zonal means shown in Figure 11 show both methods capture similar seasonal variations but a notable bias exists at all latitudes between P_H and ECMWF reference pressure ($P_{E)}$. The threshold test and its removal of relatively high values of P_H cause the large differences in the mid-latitudes. P_H also shows more structure in the tropical regions. Interannual variations of

the zonal mean P_H were found to be negligible and sub-monthly variations of P_H did not exceed 10% of the mean.

The bias between P_H and P_E suggest one or both estimates could be in error. This error could arise from bias in simulating T_{H6} or in computing ECMWF model temperatures. Such errors could introduce bias to the UTH values when applying the method to observations.

5.3 UTH algorithm

UTH retrievals using HIRS limb-adjusted observations from channels 6 and 12 were accomplished through the following relation taken from (1)

$$UTH = \frac{1}{P_H}\exp\left(a + bT_{12}\right) \tag{4}$$

where P_H is given in (3) and the fitted coefficients are given in Table 2. Figure 12 gives a scatter diagram of the fit constructed from the TIGR-3 profiles. Differences between Figure 12 and Figure 8h represent the additional error introduced by estimating P_0.

5.4 Error analysis

Error in computing UTH in (4) can arise from several sources. First, the training data set used to simulate HIRS brightness temperatures and UTH may not suitably represent tropical and mid-latitude conditions. Sensitivity analysis in Soden and Bretherton (1996)

indicate this error to be small compared to small-scale variations found in relative humidity. It is these small-scale variations that provide most of the random error in the UTH estimate. Random errors are a measure of the scatter in the radiance-to-humidity relationship seen in Figure 12. The rms error from that fit is given in Table 2 to be 1.3 K. This results in an uncertainty of 0.16 in UTH and exceeds the result given in Soden and Bretherton (1996) by 0.03. This uncertainty, when multiplied with UTH, gives the random error estimate for the UTH estimate from the fit.

Secondly, the radiative transfer simulations of HIRS brightness temperatures may differ from observations. Bias introduced by errors in modeling P_H and $T_{6.7}$ could introduce an additional systematic error to the UTH retrieval. Forward modeled HIRS channel 12 brightness temperatures used here were found in Soden et al. (2000) and Garand et al. (2000) to have less than 0.5 K bias with line-by-line models. OPTRAN simulations of HIRS channel 5 (similar to HIRS 4 and 6) were also found to not exceed 0.5 K in Garand et al. (2000). A sensitivity analysis of the systematic errors arising from inaccurate simulations of the observed brightness temperatures indicates the largest absolute error for wettest profiles. Figure 13 provides curves indicating the error in UTH for a 1K systematic error in either T_{H6} or T_{H12}. Wet profiles have the greatest sensitivity to radiative transfer bias. The positive errors indicate errors in T_{H6} with the largest errors for the wettest, coldest profiles approaching 10 % per 1 K bias in T_{H6}. Errors can be even more severe for warm, wet profiles if T_{H12} simulations are biased. These errors approach 15% for a 1 K bias in T_{H12}. Warm and dry profiles have least amount of error as is shown for the T_{H12}=265 K curve for the T_{H6} sensitivity analysis.

6. Conclusions

This study assesses the analytic expression used to compute UTH from T_{H12} observations. A summary of our assessment is:

1. Vertically averaging relative humidity with UTH weights is better in the tropics than weights based on transmission weights. Transmission weights cause a wet UTH bias for the extremely dry tropical profiles.
2. UTH weights may be inappropriate for some mid-latitude profiles because these weights average data over broad vertical regions that lie outside of the upper troposphere. The temperature lapse rate decreases significantly for colder mid-latitude profiles. For HIRS observations, we recommend removing observations with $P_0 > 1.7$ by only accepting profiles where $T_{H6}-T_{H4} > 20$ K.
3. β varies more with latitude than is shown in Soden and Bretherton (1996). This is likely due to differences in the profiles used between the studies. However, β gives highly scattered results for the coldest mid-latitude profiles due to large vertical gradients in β for mid-latitude profiles.
4. P_0 best accounts for the temperature sensitivity of the T_{H12} observations.
5. Systematic absolute error between simulated and observed brightness temperatures is greatest for the relatively warm and wet profiles with errors on the order of 15 % in UTH for 1 K error in simulating either T_{H6} or T_{H12}.

UTH retrievals are very important for model evaluation and comparison to satellite observations. Model profiles of temperature and water vapor can be inverted into HIRS channel 12 brightness temperature through a radiative transfer model. UTH data can then be constructed from model profile and satellite observations and serve as a consistent method of comparison. This means of comparison greatly reduces the impact of tuning parameters (a,b,P_H) when interpreting differences between model and observations.

Large biases can occur between different methods and different satellite estimates of UTH (Escoffier, 2000). These differences, however, do not represent a fundamental limitation on the use of UTH for climate studies, but reflect the need for satellite intercalibration, UTH validation, and UTH methodology comparison. We have investigated the methodology problem in this study. Other investigations are beginning to better quantify the calibration and intercalibration of upper tropospheric water vapor channels on different satellites [Breon et al., 1999; Breon et al., 2000; Sohn, 2000). Only when all these sources of bias are accounted for will it be possible to assess the true accuracy of UTH retrievals from different data sources.

7. Acknowledgments

We would like to thank Dr. Brian Soden for suggesting a method for computing P_0 using HIRS temperature observations and providing temperature data from ECMWF analysis. We would also would like to thank three anonymous reviewers for their constructive comments.

8. References

Bates, J.J., D.L. Jackson, F.-M. Breon, and Z.D. Bergen, Variability of tropical upper tropospheric humidity 1979-1998, *J. Geophys. Res*., accepted, 2001.

Bates, J.J., X. Wu, and D.L. Jackson, Interannual variability of upper-tropospheric water vapor band brightness temperature, *J. Climate*, **9**, 427-438, 1996.

Bates, J.J., and D.L. Jackson, A comparison of water vapor observations with AMIP I simulations, *J. Geophys Res.*, **102**, 21,837-21,852, 1997.

Berk, A., L.S. Bernstein, and D.C. Robertson, MODTRAN: A moderate resolution model for LOWTRAN 7, Spectral Sciences, Inc. 99 South Bedford St., 7 Burlington, MA 01803, 1989.

Breon, F.-M., D.L. Jackson, and J.J. Bates, Evidence of atmospheric contamination on the measurement of the spectral response of GMS-5 water vapor channel, *J. Atmos. Oceanic Technol*., **16**, 1851-1853, 1999.

Breon, F.-M.., D.L. Jackson, and J.J. Bates, Calibration of the Meteosat water vapor channel using collocated NOAA/HIRS 12 measurements, *J. Geophys. Res*., **105**, 11,925-11933, 2000.

Chaboureau, J.-P., A. Chedin, and N.A. Scott, Remote sensing of the vertical distribution of atmospheric water vapor from the TOVS observations: Method and validation, *J. Geophys. Res*, **103**, 8743-8752, 1998.

Escoffier, C., J.J. Bates, J. Schmetz, and A. Chedin, Comparison of Upper Tropospheric Humidity Retrievals from TOVS and METEOSAT, *J. Geophys. Res*., in press, 2000.

Garand, L. and co-authors, Radiance and Jacobian intercomparison of radiative transfer models applied to HIRS and AMSU channels, *J. Geophys. Res*., accepted, 2001.

Jedlovec, G.J., J.A. Lerner, and R.J. Atkinson, A satellite-derived upper-tropospheric water vapor transport index for climate studies, *J. Appl. Meteor.*, **39**, 15-41, 2000.

McMillin, L.M., L.J. Crone, and T.J. Kleespies, Atmospheric transmittance of an absorbing gas, 5. Improvements to the OPTRAN approach, *Appl. Opt*., **34**, 8396-8399, 1995.

Schmetz, J., W.P. Menzel, C. Velden, X. Wu, L. Berg, S. Nierman, C. Hayden, K. Holmlund, and C. Geijo, Monthly mean large-scale analysis of upper-tropospheric humidity and wind field divergence derived from three geostationary satellites, *Bull. Amer. Meteor. Soc.*, **76**, 1578-1584, 1995.

Soden, B.J., S.A. Ackerman, D.O'C. Starr, S.H. Melfi, and R.A. Ferrare, Comparison of upper tropospheric water vapor from GOES, Raman lidar, and cross-chain loran atmospheric sounding system measurements, *J. Geophys. Res*., **99**, 21,005-21,016, 1994.

Soden, B.J., and F.P. Bretherton, Upper tropospheric relative humidity from the GOES 6.7 μm channel: Method and climatology for July 1987, *J. Geophys. Res*., **98**, 16,669-16,688, 1993.

Soden, B.J., and F.P. Bretherton, Evaluation of water vapor distribution in general circulation models using satellite observations, *J. Geophys. Res*., **99**, 1187-1210, 1994.

Soden, B.J., and F.P. Bretherton, Interpretation of TOVS water vapor radiances in terms of layer-average relative humidities: Method and climatology for the upper,middle and lower troposphere, *J. Geophys. Res*., **101**, 9333-9343, 1996.

Soden, B.J., and R. Fu, A satellite analysis of deep convection, upper-tropospheric humidity, and the greenhouse effect, *J. Climate*, **8**, 2333-2351, 1995.

Soden, B.J. and Coauthors, An intercomparison of radiation codes fro retrieving upper-tropospheric humidity in the 6.3-μm band: A report from the first GvaP workshop, *Bull. Amer. Meteor. Soc.*, **81**, 797-808, 2000.

Sohn, B.J., J. Schmetz, S. Tjemkes, M. Koenig, H. Lutz, A. Arriaga, and E.S. Chung, Intercalibration of the Meteosat-7 water vapor channel with SSMT/2, *J. Geophys. Res*., **105**, 15,673-15,680, 2000.

Spencer, R.W., and W.D. Braswell, How dry is the tropical free troposphere? Implications for global warming theory, *Bull. Amer. Meteor. Soc.*, **78**, 1097-1106, 1997.

Stephens, G.L., D.L. Jackson, and I. Wittmeyer, Global observations of upper-tropospheric water vapor derived from TOVS radiance data, *J. Climate*, **9**, 305-326, 1996.

Susskind, J., P. Piraino, L. Rokke, L. Iredell, and A. Mehta, Characteristics of the TOVS Pathfinder Path A dataset, *Bull. Amer. Meteor. Soc*., **78**, 1449-1472, 1997.

Wang, J. G.P. Anderson, H.E. Revercomb, and R.O. Knuteson, Validation of FASCOD3 and MODTRAN3: comparison of model calculations with ground-based and airborne interferometer observations under clear-sky conditions, *Applied Optics*, **35**, 6028-6040, 1996.

8. Figure Captions

Figure 1: Mean vertical profiles of UTH weights averaged for three TIGR-3 climate zones: Tropical (TROP), mid-latitude 1 (MIDL-1) and mid-latitude 2 (MIDL-2). Solid curve is the mean and dotted curve is one standard deviation. Dashed line indicates the mean P_0 for that climate zone and the dashed-dotted line is one standard deviation.

Figure 2: Same as figure 1 except using transmission weights.

Figure 3: Same as figure 1 except using temperature.

Figure 4: Same as figure 1 except using relative humidity.

Figure 5: Same as figure 1 except using dimensionless lapse rate parameter β.

Figure 6: Scatter diagrams relating T_{H12} to UTH for three TIGR-3 climate zones using UTH weights for column 1 and transmission weights for column 2. Lines give linear least square fit with coefficients a and b indicating the intercept and slope of the fit. r is the linear correlation and rms is the root mean square error.

Figure 7: Vertical profiles of UTH (solid) and transmission (dotted) weighting profiles for a TIGR-3 tropical profile that is a) moist and b) dry in the upper troposphere.

Figure 8: Scatter diagrams in similar format as figure 6. Method 1 indicates the Stephens et al. (1996) method for column 1 diagrams and method 2 indicates the Soden and Bretherton (1996) method for column 2 diagrams. All diagrams use UTH weights for vertical averaging.

Figure 9: Scatter diagram of difference between simulated T_{H6} and T_{H4} values for the 1614 TIGR-3 tropical and mid-latitude profiles.

Figure 10: Results of fitting P_0 to the simulated HIRS channel 6 brightness temperatures. (a) TIGR-3 profiles where T_{H6}-T_{H4} > 20K, and (b) TIGR-3 profiles where T_{H6}-T_{H4} < 20 K.

Figure 11: Zonally averaged P_0 values when computed from HIRS channel 6 temperature data (1979-98) and ECMWF model data (5-year climatology) for January and July.

Figure 12: Scatter diagram relating UTH to simulated HIRS channel 12 brightness temperatures for TIGR-3 profiles. Line indicates linear least squares fit.

Figure 13: UTH sensitivity curves for systematic difference between modeled and observed brightness temperatures. T_b represents T_{H6} for the positive valued curves and T_{H12} for the negative valued curves.

9. Tables

Table 1: Weights for computing $<RH>_U$. Taken from Soden and Bretherton (1996).

Temperature level (K)	Weights
220	0.06
230	0.14
240	0.23
250	0.25
260	0.20
270	0.09
280	0.03
290	0.00

Table 2: Value of fitted parameters for UTH algorithm using HIRS observations. UTH_w and UTH_i are computed with respect to water and ice respectively.

	a	b (K^{-1})	RMS Error
UTH_w	33.353	-0.123	1.3 K
UTH_i	34.161	-0.126	1.1 K
P_H	10.329	-0.036	0.100

10. Figures

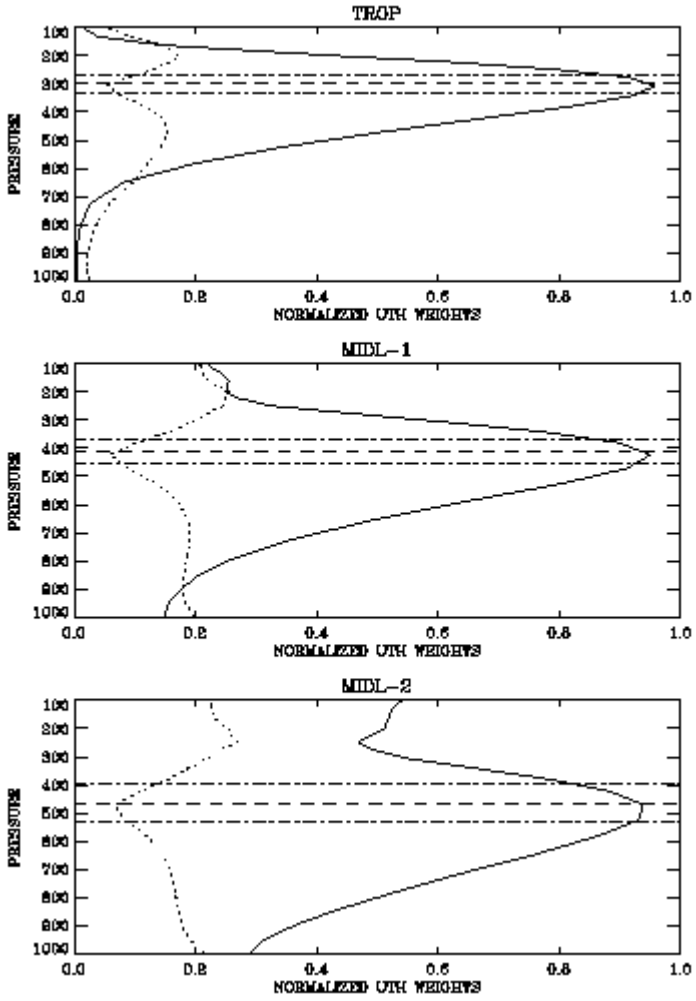

Figure 1:

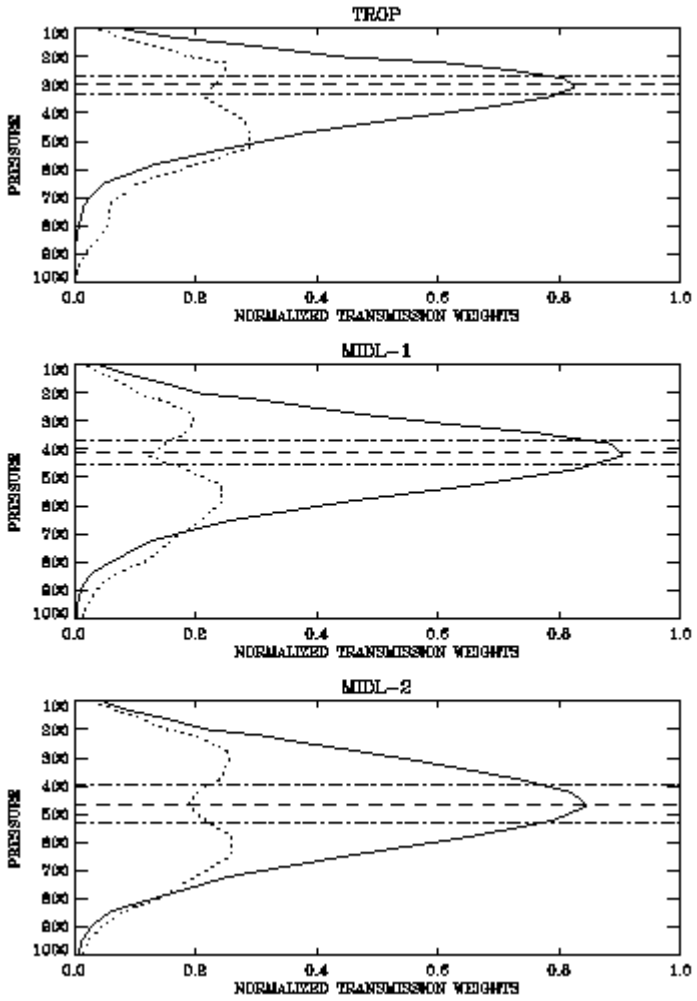
TROP
MIDL-1
MIDL-2
PRESSURE
NORMALIZED TRANSMISSION WEIGHTS
100
200
300
400
500
600
700
800
900
1000
0.0
0.2
0.4
0.6
0.8
1.0

Figure 2:

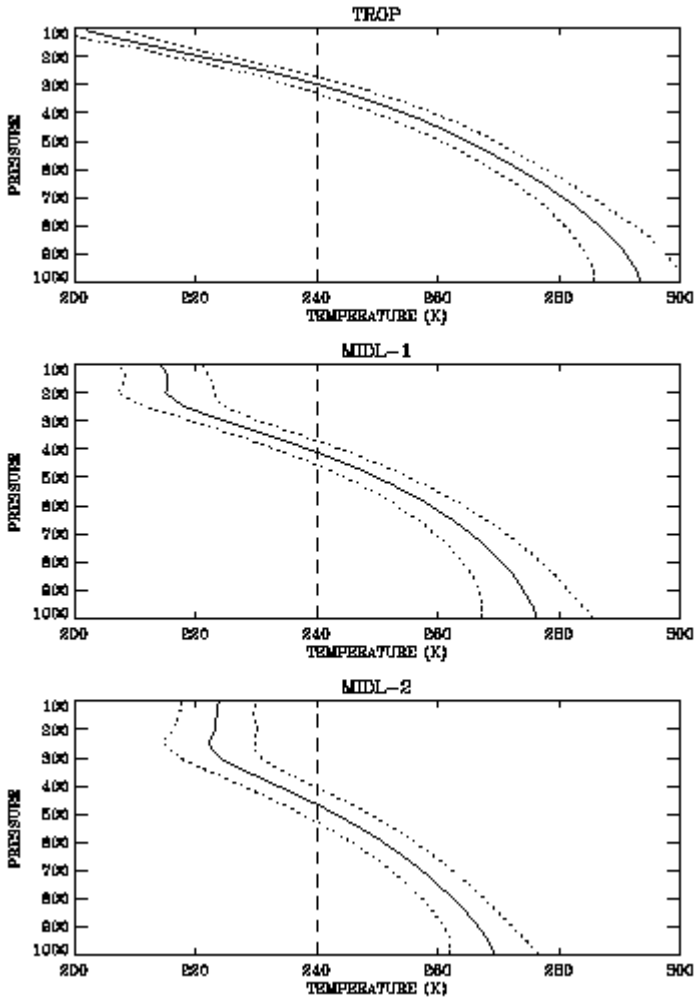
TROP
PRESSURE
100
200
300
400
500
600
700
800
900
1000
200
220
240
260
280
300
TEMPERATURE (K)
MIDL-1
PRESSURE
TEMPERATURE (K)
MIDL-2
PRESSURE
TEMPERATURE (K)

Figure 3:

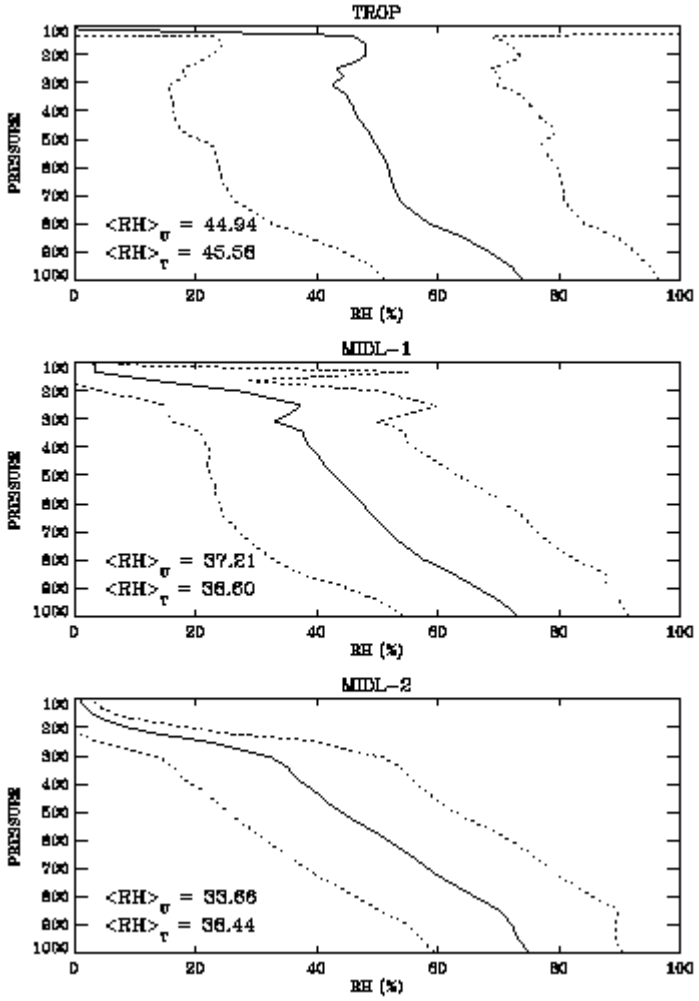
TROP
PRESSURE
<RH>σ = 44.94
<RH>τ = 45.56
RH (%)
MIDL-1
PRESSURE
<RH>σ = 37.21
<RH>τ = 36.60
RH (%)
MIDL-2
PRESSURE
<RH>σ = 33.66
<RH>τ = 36.44
RH (%)

Figure 4:

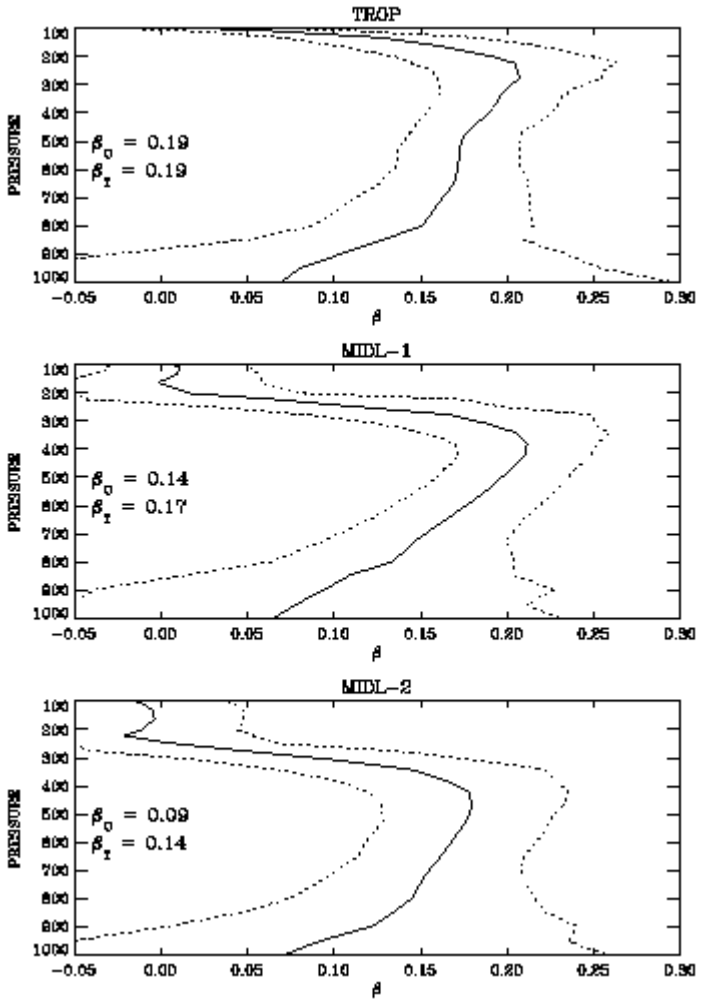
TROP
PRESSURE
100
200
300
400
500
600
700
800
900
1000
β_0 = 0.19
β_r = 0.19
−0.05
0.00
0.05
0.10
0.15
0.20
0.25
0.30
β
MIDL−1
β_0 = 0.14
β_r = 0.17
MIDL−2
β_0 = 0.09
β_r = 0.14

Figure 5:

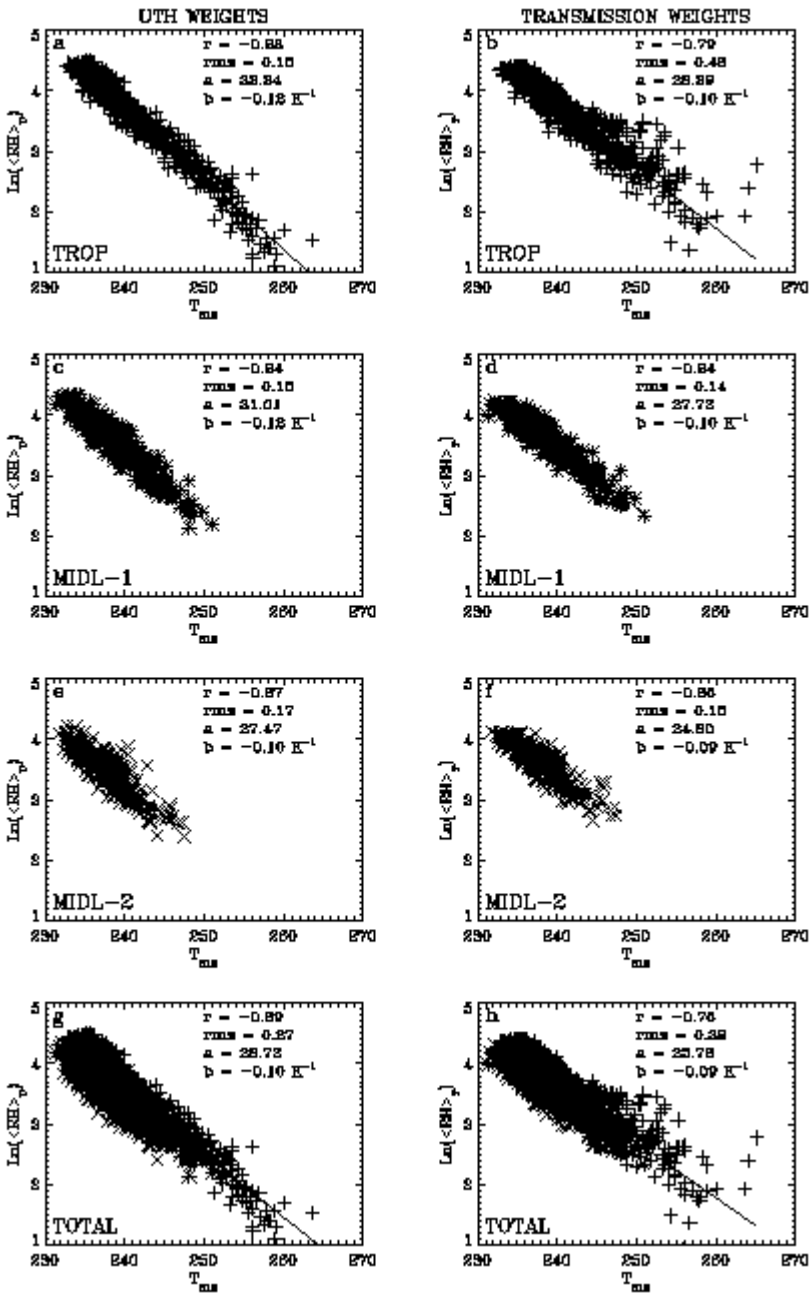
UTH WEIGHTS
TRANSMISSION WEIGHTS
a
r = −0.88
rms = 0.15
a = 38.84
b = −0.18 K⁻¹
TROP
b
r = −0.79
rms = 0.48
a = 28.89
b = −0.10 K⁻¹
TROP
c
r = −0.84
rms = 0.15
a = 31.01
b = −0.18 K⁻¹
MIDL−1
d
r = −0.84
rms = 0.14
a = 27.72
b = −0.10 K⁻¹
MIDL−1
e
r = −0.87
rms = 0.17
a = 27.47
b = −0.10 K⁻¹
MIDL−2
f
r = −0.86
rms = 0.15
a = 24.80
b = −0.09 K⁻¹
MIDL−2
g
r = −0.89
rms = 0.27
a = 28.72
b = −0.10 K⁻¹
TOTAL
h
r = −0.76
rms = 0.38
a = 25.78
b = −0.09 K⁻¹
TOTAL

Figure 6:

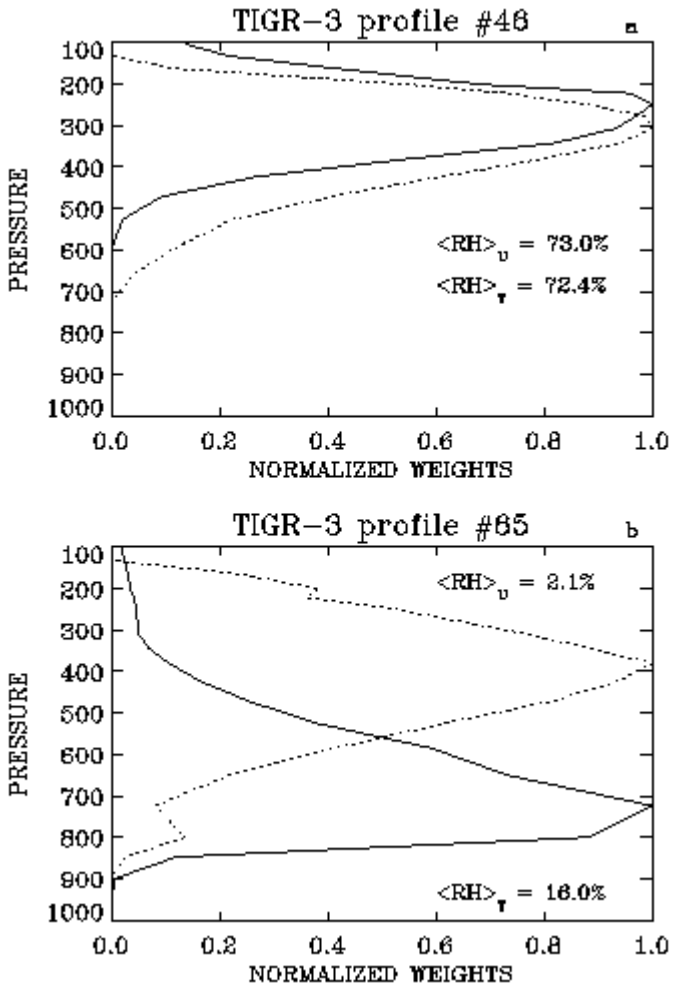
TIGR−3 profile #46
a
PRESSURE
100
200
300
400
500
600
700
800
900
1000
0.0
0.2
0.4
0.6
0.8
1.0
NORMALIZED WEIGHTS
<RH>υ = 73.0%
<RH>τ = 72.4%
TIGR−3 profile #65
b
PRESSURE
NORMALIZED WEIGHTS
<RH>υ = 2.1%
<RH>τ = 16.0%

Figure 7:

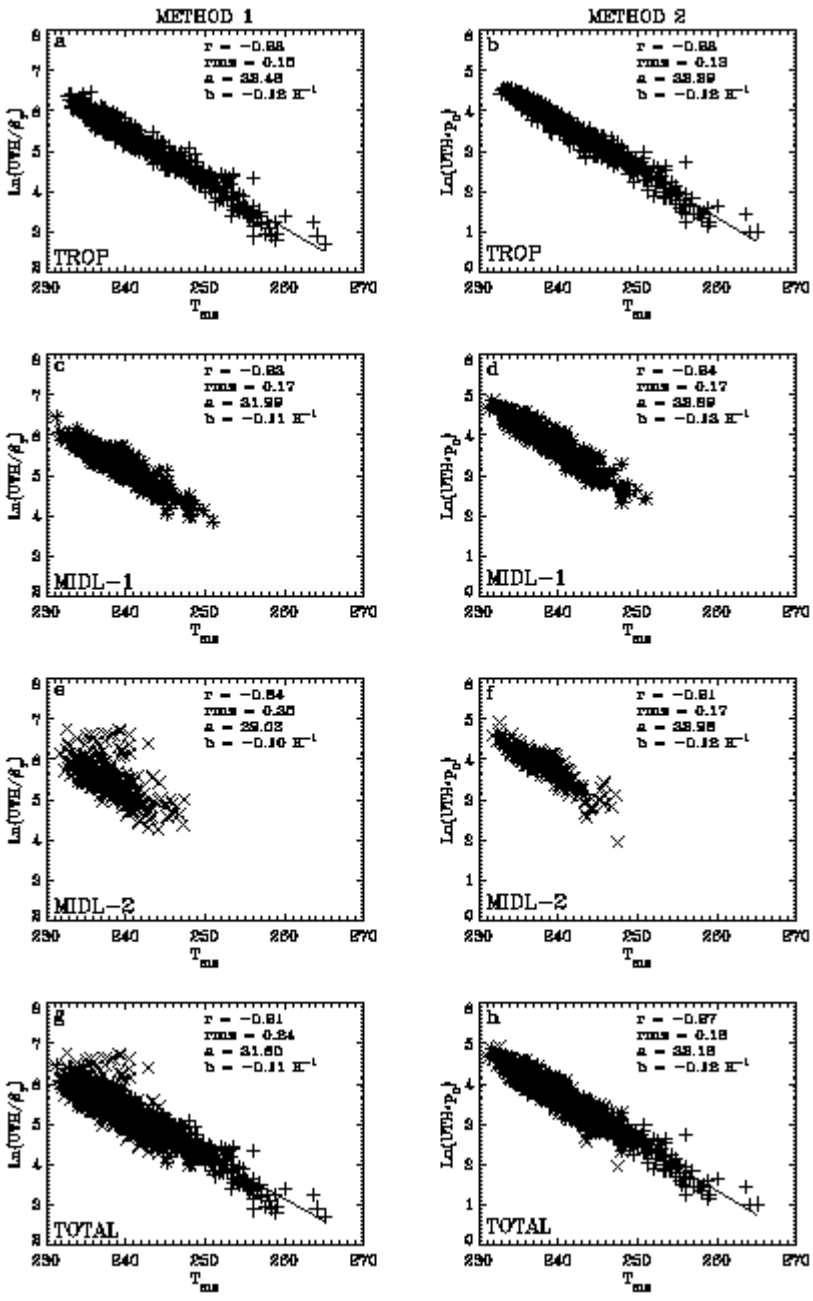
METHOD 1
METHOD 2
a
r = −0.88
rms = 0.15
a = 38.48
b = −0.12 K⁻¹
TROP
b
r = −0.88
rms = 0.13
a = 38.89
b = −0.12 K⁻¹
TROP
c
r = −0.83
rms = 0.17
a = 31.99
b = −0.11 K⁻¹
MIDL−1
d
r = −0.84
rms = 0.17
a = 38.89
b = −0.13 K⁻¹
MIDL−1
e
r = −0.84
rms = 0.25
a = 29.02
b = −0.10 K⁻¹
MIDL−2
f
r = −0.81
rms = 0.17
a = 38.98
b = −0.12 K⁻¹
MIDL−2
g
r = −0.81
rms = 0.24
a = 31.60
b = −0.11 K⁻¹
TOTAL
h
r = −0.87
rms = 0.13
a = 38.18
b = −0.12 K⁻¹
TOTAL
290
240
250
260
270

Figure 8:

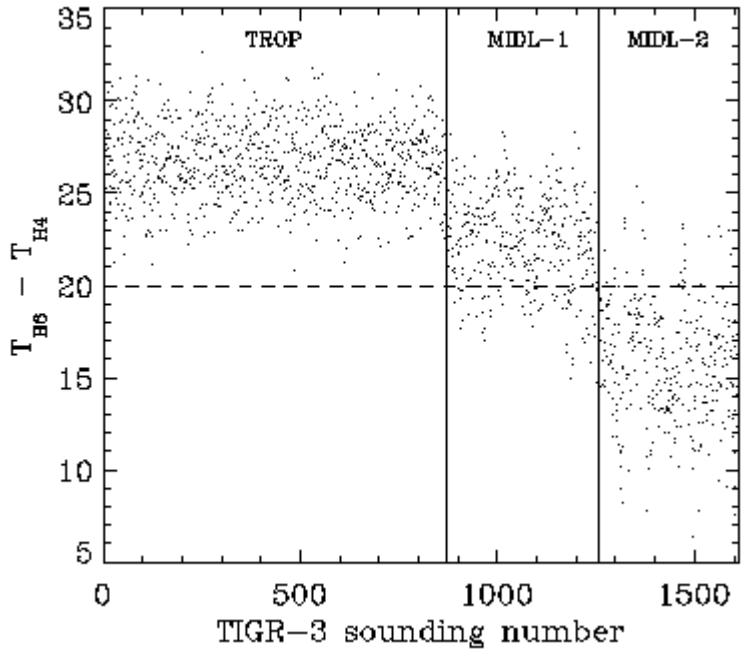

Figure 9:

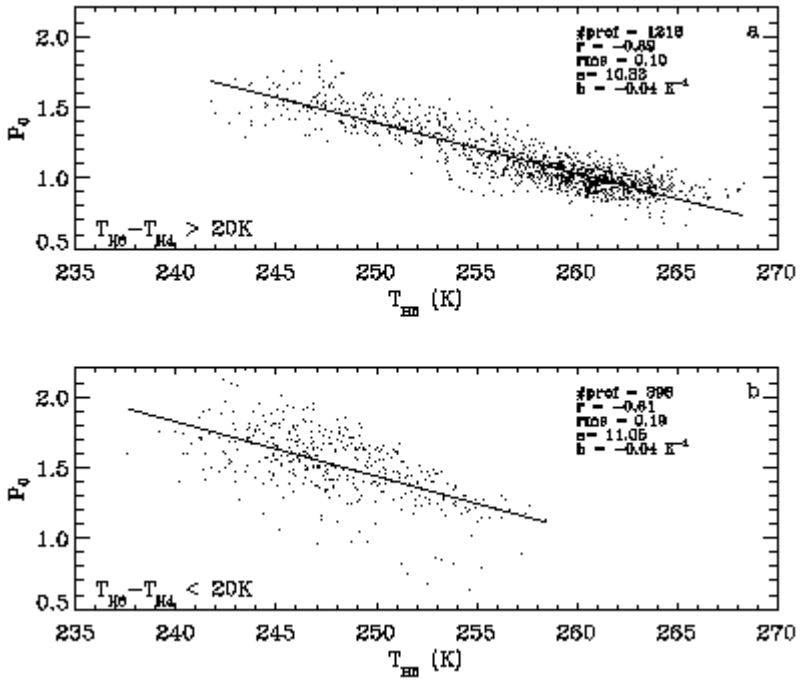

Figure 10:

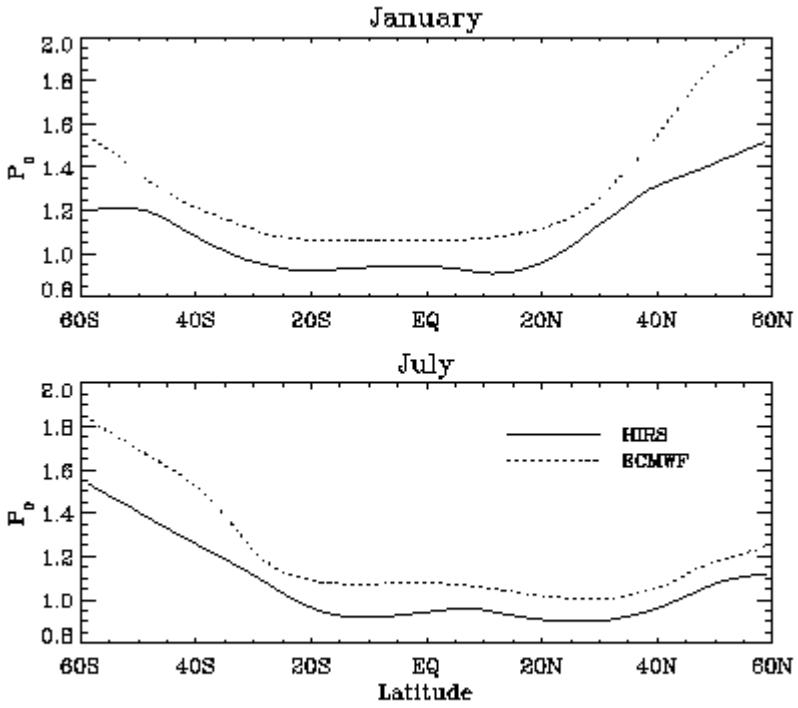
January
2.0
1.8
1.6
1.4
1.2
1.0
0.8
P_b
60S
40S
20S
EQ
20N
40N
60N
July
HIRS
ECMWF
Latitude

Figure 11:

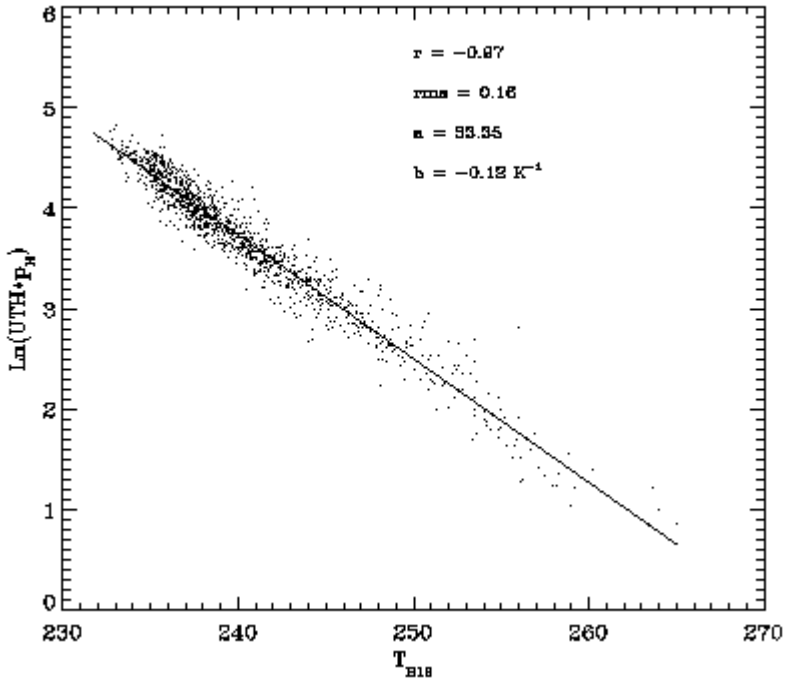
r = −0.97
rms = 0.16
a = 33.35
b = −0.12 K⁻¹
Ln(UTH·P_H)
T_B18
0
1
2
3
4
5
6
230
240
250
260
270

Figure 12:

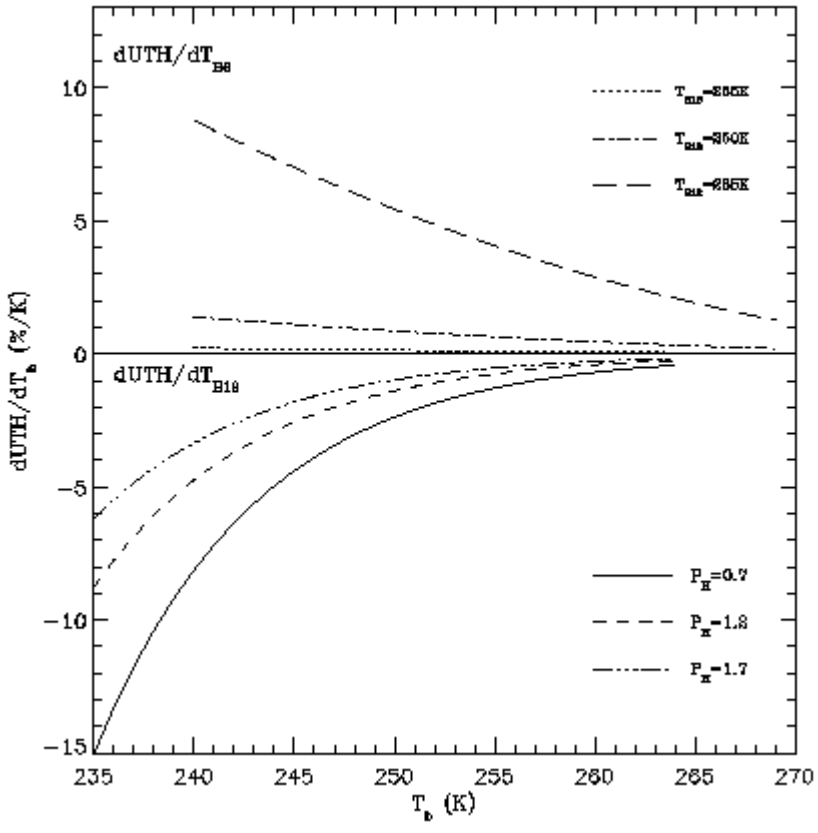

Figure 13: